nature neuroscience

Coordinated grid and place cell replay during rest

H Freyja Ólafsdóttir[1], Francis Carpenter[1,2] & Caswell Barry[1]

Hippocampal replay has been hypothesized to underlie memory consolidation and navigational planning, yet the involvement of grid cells in replay is unknown. During replay we found grid cells to be spatially coherent with place cells, encoding locations 11 ms delayed relative to the hippocampus, with directionally modulated grid cells and forward replay exhibiting the greatest coherence with the CA1 area of the hippocampus. This suggests grid cells are engaged during the consolidation of spatial memories to the neocortex.

© 2016 Nature America, Inc. All rights reserved.

npg

During exploration, the activity of place[1] and grid cells[2] represents self-location. Together these cells have been hypothesized to support spatial memory[1,3] and navigation[3,4]. Hippocampal replay[5,6]—the reactivation of place cell sequences during immobility and sleep—has been proposed as a mechanism for consolidation[5] and route planning[7], yet the involvement of grid cells remains unknown. Potentially, spatially coherent place and grid cell activity may emerge during replay as the hippocampus broadcasts memory traces to the cortex[8]. To study the involvement of grid cells in replay we recorded concurrently from rodent medial entorhinal cortex (MEC) layers V and VI (V/VI) and hippocampus (CA1) during track-running and subsequent rest. We report robust coherence between place and grid cell spatial representations during hippocampal replay.

We recorded a total of 43 grid cells across 11 sessions from 6 rats concurrently with 34–72 place cells in each session, for a total of 592 place cells (**Fig. 1a–d**, **Supplementary Figs. 1** and **2** and **Supplementary Table 1**). During subsequent rest, we identified putative replay events on the basis of place cell activity (**Fig. 1e** and Online Methods). We used a Bayesian decoding algorithm[9] and a trajectory-fitting procedure to reconstruct position and score the replay[9] (**Supplementary Fig. 3**). For further analyses, we used robust replay events exhibiting clear, straight trajectories (each $P < 0.2$ versus their own shuffle). On average, grid cell activity was higher during replay events than during non-replay periods[10] (2.19 Hz (s.d. = 1.74) versus 1.33 Hz (s.d. = 1.61), $t_{(43)} = 3.24$, $P = 0.00023$), with peak grid cell activity lagging that of place cells by 10 ms (**Fig. 1f** and **Supplementary Fig. 4**). To investigate grid–place cell spatial coherence, we assessed the similarity of the grid and place cell representations during replay events in which both were active. Specifically, we superimposed the trajectory derived from a hippocampal replay event onto the decoded representation from concurrently recorded grid cell spikes (**Supplementary Fig. 5**). The position represented by grid cells during replay events was similar to that represented by the place cell trajectories (**Fig. 2a** and **Supplementary Fig. 6**), exceeding the coherence obtained by pairing a grid cell event with a random place cell event from the same session ($P < 0.0001$, area under the curve (AUC) test; Online Methods, **Fig. 2b** and **Supplementary Fig. 5**); comparisons against

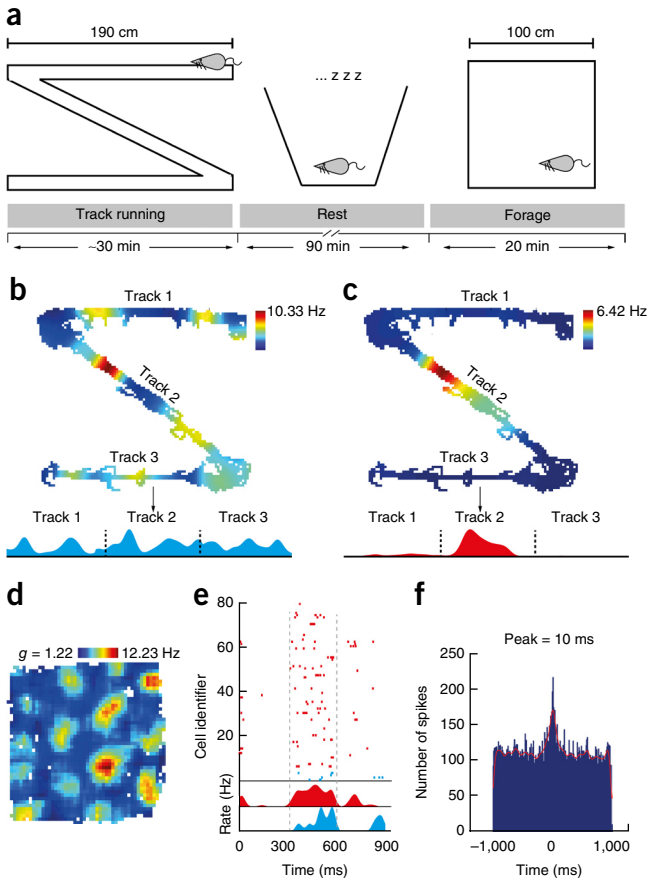

Figure 1 Experimental procedure. (**a**) Rats ran 20 laps on a Z-shaped track (Track Running) and were then placed in a rest enclosure (Rest) for an hour and a half and finally completed an open field foraging session (Forage). (**b**,**c**) Replay analyses were based on linearized track ratemaps. The grid (**b**) and place (**c**) cells from a single example are shown. (**d**) Open field ratemaps were used to identify grid and directionally modulated cells (example grid cell shown; g is the gridness). (**e**) Example event. Top, raster plot of place cell (red, 0–700 Hz) and grid cell (blue, 0–300 Hz) spikes recorded during rest. Dashed vertical lines mark start and end of replay event (*x* axis, time; *y* axis, arbitrary cell IDs). Bottom, smoothed multi-unit place (red) and grid (blue) activity (*x* axis, time; *y* axis, spike rate in Hz). **(f)** Peristimulus time histogram (PSTH) of grid cell activity during replay events, centered on the middle of the event (*x* axis, time; *y* axis, number of spikes; red line, smoothed spike number).

[1]Department of Cell and Developmental Biology, University College London, London, UK. [2]Institute of Neurology, University College London, London, UK. Correspondence should be addressed to H.F.O. (h.olafsdottir@ucl.ac.uk) or C.B. (caswell.barry@ucl.ac.uk).

Received 18 February; accepted 24 March; published online 18 April 2016; doi:10.1038/nn.4291

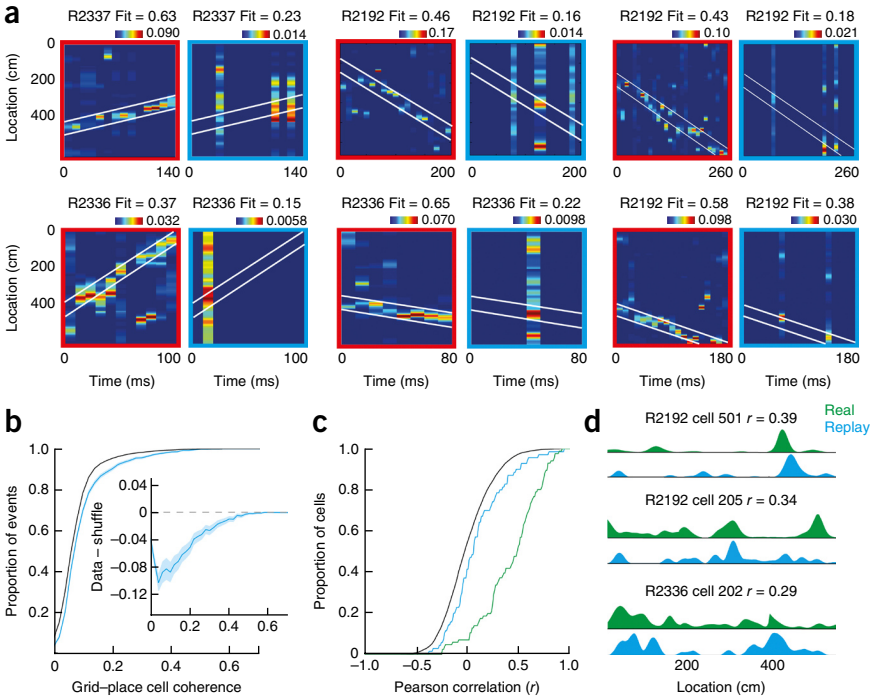

Figure 2 Grid–place cell spatial coherence during replay. (**a**) Six example reconstructed replay events based on concomitant place cell (red boxes) and grid cell (blue boxes) spikes (*x* axis, time; *y* axis, linearized position). White lines mark the extent of the line-fit based on place cell activity. Title indicates animal ID and strength of line-fit (proportion of probability matrix within the fitted line). Top row left: 2 grid cells, 3 spikes; middle: 3 grid cells, 4 spikes; right: 3 grid cells, 3 spikes. Bottom row left: 1 grid cell, 1 spike; middle: 1 grid cell, 1 spike; right: 2 grid cells, 2 spikes. (**b**) Bootstrapped cumulative distribution of grid–place coherence (place cell line-fit imposed on grid cells) obtained for all animals (blue line); shaded area shows 1 s.d. (*x* axis, coherence scores; *y* axis, cumulative proportion of events). Black line shows distribution from shuffle (random pairing of grid and place cell events). Inset: difference between data and shuffle; negative difference indicates greater coherence in the data distribution. (**c**) Cumulative distribution of correlations between track and event ratemaps for grid cells (blue line; *x* axis, Pearson correlation (r); *y* axis, proportion of grid cells), distribution from shuffle (black line; event and track ratemaps correlated at all lags) and distribution of correlations between track ratemap and ratemaps derived from position decoded from place cell activity during track running (green line). (**d**) Three example track (green) and event (blue) ratemaps. Peak values are, from top to bottom, 25.44 Hz, 0.944 Hz, 2.58 Hz, 0.408 Hz, = 4.32 Hz and 0.290 Hz.

shuffled distributions generated by permuting grid cell ratemaps ($P < 0.0001$ AUC) and spike times ($P < 0.001$ AUC) corroborated this finding (**Supplementary Figs. 7** and **8**). Grid–place cell coherence also exceeded chance levels when analysis was limited to just the strongest ($P < 0.025$ versus their own shuffle) place cell replay events ($P < 0.0001$ AUC, **Supplementary Fig. 9**) and did not exceed chance levels for the least robust ($P > 0.5$) place cell events ($P = 0.17$ AUC, **Supplementary Fig. 10**).

To confirm these results, we constructed an 'event ratemap' for each grid cell using the spikes emitted during replay events and the position decoded from concurrent place cell activity (see Online Methods). Event ratemaps and ratemaps generated from track running were similar (mean Pearson correlation $r = 0.10$, s.e.m. = 0.033, **Fig. 2c,d**) and exceeded the correlations obtained from two shuffling procedures (ratemap shuffle $W_{(78)} = 763$, $P = 0.0079$; grid spike times shuffle, $W_{(78)} = 703$, $P = 0.01$). In summary, we employed two distinct methods to assess spatial coherence between grid and place cells during replay events, confirming that these cell types are closely coordinated during hippocampal replay.

Forward replay—i.e., events that preserve place field sequences experienced during wakefulness—has been linked to consolidation and planning[5,7] and reverse replay to reward learning[6]. Consequently, we assessed coordination between grid and place cells during forward and reverse replay events separately. Grid cells were more likely to be active during forward than reverse events (forward, 639 of 1,127 (57%); reverse, 315 of 699 (45%); $\chi^2 = 23.41$, $P < 0.0001$) and grid–place cell spatial coherence was greater for forward than reverse replay ($P = 0.0006$ AUC, **Fig. 3a**). This difference did not result from the unequal number of forward and reverse events: equating the number of events by down-sampling did not eliminate the difference

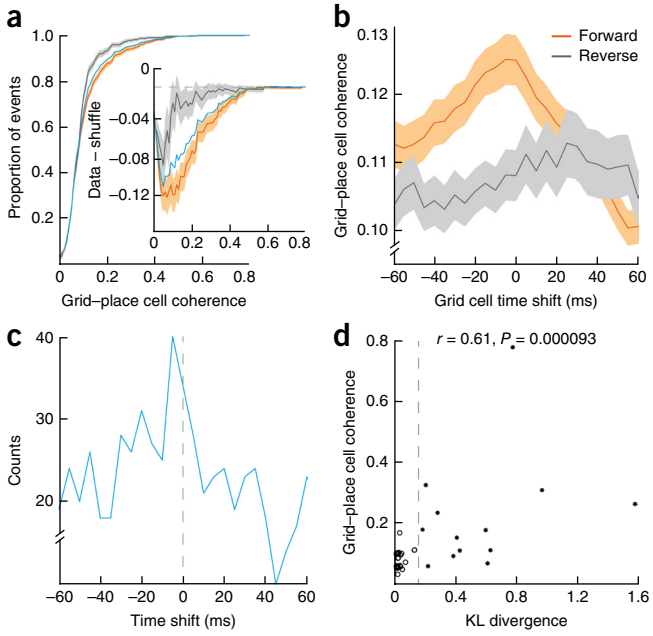

Figure 3 Grid–place cell coherence is stronger for forward replay and directionally modulated cells. (**a**) Bootstrapped cumulative distribution of spatial coherence scores for forward (orange), reverse (gray) and both (blue) replay events; shaded area, 1 s.d. (*x* axis, grid–place cell coherence; *y* axis, cumulative proportion of events). Inset, difference between data and shuffle. (**b**) Mean grid–place cell coherence versus time shift of grid cell spikes for forward (orange) and reverse (gray) events (*x* axis, grid cell time shift (negative indicates that grid spikes were moved back in time relative to place cell spikes); *y* axis, mean grid–place coherence; shaded areas, s.e.m.). (**c**) Distribution of time shift associated with highest grid–place cell coherence (*x* axis, grid cell time shift; *y* axis, number of events). (**d**) Grid–place cell coherence as a function of grid cell directional modulation (*x* axis, KL divergence of each grid cell; *y* axis, mean spatial coherence with place cells during replay using Spearman rank order correlation; open circles, grid cells with KL <0.15; black points, grid cells with KL ≥0.15).

© 2016 Nature America, Inc. All rights reserved.

($P < 0.0001$). Forward and reverse events both exhibited grid–place cell coherence that significantly exceeded chance levels (forward, $P < 0.0001$ AUC; reverse, $P = 0.0093$ AUC; **Fig. 3a**).

Next, we examined the temporal relationship between grid and place cell spatial coherence during replay events. If grid cell participation in replay results from a consolidation mechanism[5], the location encoded by grid cells might lag the place cell trajectory, as in the 10-ms lag seen in peak rates between the two regions (**Fig. 1f**). We investigated grid–place cell coherence for time lags between ±60 ms, finding a significant effect of time for forward but not reverse events (forward, $F_{(24,4320)} = 9.26$, $P < 0.0001$; reverse, $F_{(24,1464)} = 0.37$, $P = 0.75$). Moreover, for forward events we found the highest grid–place cell coherence when grid cell spike times were shifted back by an average of 11 ms relative to place cells (**Fig. 3b**). Analysis of the distribution of best time shifts across forward events revealed a unimodal distribution peaking at 8 ms (**Fig. 3c**).

Finally, we investigated the relationship between the strength of replay coherence for individual grid cells (indexed by their mean spatial coherence) and the extent of their modulation by head direction and hexagonal symmetry in the open field (gridness[11]). We found that directional modulation correlated with replay coherence (Spearman's $r = 0.61$, $P = 0.000093$, **Fig. 3d**) such that directional grid cells (Kullback–Leibler (KL) divergence > 0.15)[12] exhibited higher coherence with place cells than nondirectional grid cells (0.16 (s.d. = 0.082) versus 0.082 (s.d. = 0.030), $t_{(35)} = 3.57$, $P = 0.0011$, $P < 0.0001$ AUC test). Yet both cell types showed significant grid–place cell coherence (directional cells: $P < 0.0001$ AUC, nondirectional cells: $P < 0.0001$ AUC, **Supplementary Fig. 11**), as well as a lag relative to the CA1 encoded location (directional cells, $F_{(24,1056)} = 4.150$, $P < 0.0001$; nondirectional cells, $F_{(24,3312)} = 3.060$, $P < 0.0001$; **Supplementary Fig. 12**). Grid–place cell coherence was not modulated by hexagonal symmetry (Spearman's $r = 0.14$, $P = 0.41$, **Supplementary Fig. 13**).

To conclude, we report that hippocampal place cells and MEC V/VI grid cells (**Supplementary Fig. 14**) are closely coordinated during replay, suggesting that replay may be a general property of networks encoding self-location. Moreover, grid cells are more active during forward replay events during which they exhibit greater spatial coherence with place cells. During these events the position encoded by MEC V/VI lags behind that in CA1, suggesting that replay sequences originate in the hippocampus and propagate to the MEC. As the coordination occurs in the absence of sensory cues, it plausibly originates from the internal dynamics of the hippocampal network[13]. Together this supports the view that replay during rest is the mechanism by which memories are consolidated to the neocortex[8], MEC V/VI being the primary cortical output target of the hippocampus. It remains to be seen whether grid cells in superficial MEC are engaged during on-track replay or navigational planning[4].

METHODS

Methods and any associated references are available in the online version of the paper.

Note: Any Supplementary Information and Source Data files are available in the online version of the paper.

ACKNOWLEDGMENTS

This work was supported by the Wellcome Trust and the Royal Society (101208/Z/13/Z). The authors thank N. Burgess, K. Jeffery, T. Wills, D. Bush and A. Saleem for comments on the manuscript.

AUTHOR CONTRIBUTIONS

H.F.Ó. and C.B. conceived of the project jointly. H.F.Ó. and F.C. performed surgeries. H.F.Ó. carried out the experiments. H.F.Ó. and C.B. performed the analyses. All authors wrote the manuscript.

COMPETING FINANCIAL INTERESTS

The authors declare no competing financial interests.

Reprints and permissions information is available online at http://www.nature.com/reprints/index.html.

1. O'Keefe, J. & Nadel, L. *The Hippocampus as a Cognitive Map* (Claredon, Oxford, 1978).
2. Hafting, T., Fyhn, M., Molden, S., Moser, M.B. & Moser, E.I. *Nature* **436**, 801–806 (2005).
3. McNaughton, B.L., Battaglia, F.P., Jensen, O., Moser, E.I. & Moser, M.B. *Rev. Neurosci.* **7**, 663–678 (2006).
4. Bush, D., Barry, C., Manson, D. & Burgess, N. *Neuron* **87**, 507–520 (2015).
5. Wilson, M.A. & McNaughton, B.L. *Science* **265**, 676–679 (1994).
6. Foster, D.J. & Wilson, M.A. *Nature* **440**, 680–683 (2006).
7. Pfeiffer, B.E. & Foster, D.J. *Nature* **497**, 74–79 (2013).
8. Marr, D. *Phil. Trans. R. Soc. Lond. B* **262**, 23–81 (1971).
9. Ólafsdóttir, H.F., Barry, C., Saleem, A.B., Hassabis, D. & Spiers, H.J. *eLife* **4**, e06063 (2015).
10. Chrobak, J.J. & Buzsáki, G. *J. Neurosci.* **14**, 6160–6170 (1994).
11. Boccara, C.N. *et al. Nat. Neurosci.* **13**, 987–994 (2010).
12. Doeller, C.F., Barry, C. & Burgess, N. *Nature* **463**, 657–661 (2010).
13. Pastalkova, E., Itskov, V., Amarasingham, A. & Buzsáki, G. *Science* **321**, 1322–1327 (2008).

© 2016 Nature America, Inc. All rights reserved.

ONLINE METHODS

Animals and surgery. Six male Lister Hooded rats were used in this study. All procedures were approved by the UK Home Office, subject to the restrictions and provisions contained in the Animals (Scientific Procedures) Act of 1986. All rats (330–400 g at implantation) received two microdrives, each carrying eight tetrodes of twisted 17 µm HM-L coated platinum iridium wire (90% and 10%, respectively; California Fine Wire), targeted to the right CA1 (ML: 2.2 mm, AP: 3.8 mm posterior to bregma) and left medial entorhinal cortex (MEC) (ML = 4.5 mm, AP = 0.3–0.7 anterior to the transverse sinus, angled between 8–10°). Wires were platinum plated to reduce impedance to 200–300 k at 1 kHz. After rats had recovered from surgery they were maintained at 90% of free-feeding weight with *ad libitum* access to water and were housed individually on a 12-h light-dark cycle.

Recording. Screening was performed post-surgically after a 1-week recovery period. An Axona recording system (Axona Ltd.) was used to acquire the single-units and positional data (for details of the recording system and basic recording protocol see Barry *et al.*[14]). The position and head direction of the animals was inferred using an overhead video camera to record the location of two light-emitting diodes (LED) mounted on the animals' head-stages (50 Hz). Tetrodes were gradually advanced in 62.5 µm steps across days until place cells (CA1) or grid cells (MEC) were found.

Experimental apparatus and protocol. The experiment was run during the animals' light period, to facilitate rest during the rest session. During track running sessions animals shuttled back and forward on a Z-shaped track comprised of 10 cm wide runways covered with black paint, raised 75 cm off the ground. The two parallel sections of the Z (190 cm each) were connected by a diagonal section (220 cm). The entire track was surrounded by plain black curtains. Animals were pretrained to run on the track, taking between 3 and 6 d before they would shuttle fluently from one end to the other. At the start of each session, rats were placed at one end of the Z-track. The same end was used as a starting location for every day of the experiment and for every rat. The ends and corners of the track were baited with sweetened rice to encourage running from one end to the other. In each session rats completed 20 full laps (30–45 min).

Following the track session, rats were placed in the rest enclosure for an hour and a half. The rest enclosure consisted of a cylindrically shaped environment (18 cm diameter, 61 cm high) with a towel placed at the bottom and was located outside of the curtains that surrounded the Z-track. Animals were not able to see the surrounding room while in the rest enclosure. Prior to recording, rats had been familiarized with the rest environment for at least 7 d.

Following the rest session, rats completed a 20 min foraging trial in a familiar open field environment. Recordings made during this period provided the basis on which spatially modulated cells were functionally classified.

As we did not use experimental groups, randomization and experimenter blinding were not applicable.

Data inclusion/exclusion. Once animals were experienced and ran well on the track (following 3–6 d of training) we considered that any session with at least 30 place cells and 1 grid cell met our minimum requirements and hence was eligible for analysis. The number of sessions that fulfilled these criteria varied between animals (1–3). Importantly, if multiple sessions were included from the same animal, we ensured the different sessions did not contain the same grid cells (based on history of electrode movement, waveforms and spatial ratemaps in the open field screening sessions).

The criteria for including place and grid cells are described below in the 'Functional classification' and 'Data analysis' sections, as are the criteria for including replay events ('Data analysis' section). All data that met these criteria were included in all of the analyses.

Functional classification. We classified spatially modulated MEC cells as grid cells using a shuffling procedure similar to that applied elsewhere[15,16]. Specifically, the hexagonal regularity of each cell was assessed using two methods, the 'standard' gridness measure[17] and 'modified' gridness measure[16]. For each method the values calculated for each cell were compared with a null distribution of 100 values obtained by calculating the gridness values of data in which the cell's spike train had been randomly permuted relative to the position of the animal by at least 30 s. A cell was considered to be a grid cell and admitted to the main analysis if its standard or modified gridness value exceeded the 97.5th percentile of the matching null distribution; 43 grid cells from 6 rats were identified.

Following Doeller *et al.*[12], we assessed the extent of directional modulation exhibited by each grid cell by calculating the Kullback–Leibler (KL) divergence between the cell's polar rate map and a uniform circular distribution with equal mean:

$$D_{KL} = \sum_i \frac{\tau_1(i)\log\left(\tau_1(i)\right)}{\tau_2(i)} \quad (1)$$

where $\tau_1(i)$ is the value in the i^{th} bin of a polar rate map normalized to have area 1 (as a probability distribution) and $\tau_2(i)$ is the i^{th} bin of a uniform probability distribution with the same number of bins as τ_1. Grid cells with KL divergence greater than 0.15 were considered to be directional[12] (13 of 43 cells).

Data analysis. We generated ratemaps for runs on the Z-track after first excluding areas in which the animals regularly performed non-perambulatory behaviors (for example, eating or grooming), which generally took place in the final 10 cm at either end of the track and 5 cm around each of the two corners. Periods when the animals' running speed was less than 3 cm/s were also excluded. Each animal's path was linearized and dwell time and spikes binned into 2 cm bins, then smoothed with a Gaussian kernel ($\sigma = 5$ bins). We calculated the firing rate for each bin by dividing the spike number by dwell time. We generated separate ratemaps for runs in the outbound and inbound directions.

We identified replay events from the rest session on the basis of the activity of hippocampal place cells using a similar method to Pfeiffer and Foster[7] and Ólafsdóttir *et al.*[9] Hippocampal cells were classified as place cells if their firing field's peak firing rate exceeded 1 Hz and was at least 20 cm long. Interneurons, identified by narrow waveforms and high firing rates, were excluded from all analyses. To identify replay events, multi-unit (MU) activity from hippocampal place cells only were binned into 1 ms temporal bins and smoothed with a Gaussian kernel ($\sigma = 5$ ms). We identified periods when the MU activity exceeded the mean rate by 3 s.d. as putative replay events and determined the start and end points of each putative replay event as the time when the MU activity fell back to the mean. Events less than 40 ms long or which included activity from less than 15% of the recorded place cell ensemble were rejected (4,382 events included in total).

To analyze modulation of grid cell activity by replay events we first estimated the firing rate of each cell inside ('event rate') and outside ('baseline rate') events. Differences in event and baseline rates were then assessed using a paired *t*-test. Second, to assess the temporal synchrony between grid cell activity and replay events, we generated peristimulus time histograms (PSTH) for each event, centered on the temporal midpoint of the event (bin size = 10 ms). Specifically, for each event we counted the number of grid cell spikes emitted in a 2,000 ms window centered on the middle of the event. Spikes were then summed across all recorded events to generate one PSTH per session. Finally, PSTHs for all sessions were combined into a single grand PSTH, the peak of which was identified. The same procedure was repeated for place cells.

To analyze replay, place cell spikes from putative events were binned into 10 ms temporal bins and a Bayesian framework[9] was used to calculate the probability of the animal's presence in each spatial bin given the observed spikes (the posterior probability matrix). This approach was validated using data from the track running session except that spikes were binned into 500 ms temporal bins and location was decoded from the posterior probability matrix using a simple maximum likelihood method. Within each temporal bin the animal's location was decoded to the bin with the highest posterior probability and this was compared with the known true location (mean decoding error 20 cm). Note that we generated two posterior probability matrices for each event, one for inbound runs and one for outbound runs.

To score the extent to which putative replay events represented a constant speed trajectory along the Z-track we applied a line-fitting algorithm[9]. Lines were defined with a gradient (V) and intercept (c), equivalent to the velocity and starting location of the trajectory. We defined the goodness of fit of a given line ($R(V,c)$) as the proportion of the probability distribution that lay within 30 cm of it. Specifically where P is the probability matrix:

$$R(V,c) = \frac{1}{n}\sum_{t=0}^{n-1} P\left(\left|x(t) - (V.t.T + c)\right| \le d\right) \quad (2)$$

© 2016 Nature America, Inc. All rights reserved.

doi:10.1038/nn.4291

where t indexes the time bins of width T and d is set to 30 cm. We maximized ($R(V,c)$ using an exhaustive search to test all combinations of V between -50 ms^{-1} and 50 ms^{-1} in 0.5 ms^{-1} increments (excluding slow trajectories with speeds >-2 ms^{-1} and <2 ms^{-1}) and c between -15 m and 21 m in 0.01 m increments.

To assess putative replay events for significance we carried out a spatial shuffle of the place cell ratemaps. Specifically, each ratemap was shuffled by shifting it relative to the track by a random number of bins drawn from a flat distribution between 1 and the length of the track minus 1 bin. The ratemap for each cell was rotated independently and in each case trailing bins were wrapped around to ensure an equal number of bins were used for each shuffle. We repeated this process 100 times for each event and for each shuffle we calculated a goodness of fit measure (as described above). This enabled us to estimate the probability of obtaining a given event by chance. Robust events, with an individual P-value of less than 0.2, were accepted as replay events and submitted to further analyses (1,826 out of 4,382 putative events). Note that we generated two shuffling distributions for each event, one for inbound runs and one for outbound runs. An event was considered to be inbound run if the P-value for the inbound run was lower than that for outbound runs, and vice versa. Thus, only one event (either inbound or outbound) was submitted to further analyses. Finally, for all inbound events the grid cell ratemaps for inbound runs were used to assess grid–place cell coherence, and conversely for outbound events we used grid cell ratemaps.

To investigate spatial coherence between grid and place cells during replay events we applied the same Bayesian framework to the grid cell spikes. Hence, for each replay event we also calculated a posterior probability matrix based solely on the observed grid cell spikes. Rather than fitting straight-line trajectories to the periodic grid cell posteriors, we compared the best-fit line from the concurrently recorded place cell posterior. Specifically, we fitted a line with the same intercept and slope as the concurrent place cell event and calculated the proportion of the probability distribution lying within $0.5x$ cm of the line, where x was equal to the average size of the grid cell firing fields recorded from that animal on the linear track. This value was used to index grid–place cell replay coherence. To estimate statistical significance of the observed coherence scores we used three different shuffling procedures.

In the first instance a shuffle distribution was generated by randomly pairing each grid cell posterior with 100 non-concurrent place cell events from the same animal and from the same session; only place cell events that were also accompanied by grid cell firing were used. We then reran the line fitting procedure to estimate grid–place cell replay coherence, as described above. To assess the statistical significance of the obtained distribution of coherence scores against the shuffle we bootstrapped the data distribution 10,000 times, computing the cumulative distribution and the corresponding area under the curve (AUC, i.e., the sum of the cumulative distribution) for each bootstrap. Difference scores between each of the 10,000 AUC scores obtained from the bootstrapped data and the shuffle distribution were computed and the 95% confidence interval estimated on the basis of on these difference scores (assuming a 2-sided test). A result was deemed statistically significant if the confidence interval did not contain 0.

Second, we applied a spatial shuffling procedure. This procedure was similar to the shuffling procedure used for place cell events. Specifically, each grid cell ratemap was shuffled by shifting it relative to the track by a random number between 10 and the length of the track minus 10 bins. The ratemap for each cell was rotated independently and trailing bins were wrapped around to ensure an equal number of bins were used for each shuffle. We repeated this process 100 times for each event. For each shuffle, the grid–place cell replay coherence score was calculated using the slope and intercept parameters of the best-fit line of the accompanying place cell event (unshuffled). To assess statistical significance we used an AUC test as described above.

Third, we applied a temporal shuffling procedure. Specifically, we shifted the spike times of grid cells active in replay events by a random amount between 5 ms and the length of the event minus 5 ms. The relative timing of spikes from the same cell was maintained. Trailing spikes were wrapped around to the start of the event to ensure an equal number of spikes contributed to each shuffle. For each shuffled event, we generated its posterior probability matrix, compared it to the best-fit line from the concurrent place cell event (unshuffled) to the shuffled posterior and computed a grid–place cell replay coherence score as detailed above. Statistical significance was again assessed using an AUC test.

Finally, we employed a second, distinct approach, to validate our observation of coherence between grid and place cells during replay. Namely, for each grid cell we constructed an event ratemap by using the timing of grid cell spikes during replay events and the decoded location based on the line fit to the place cell posterior probability matrix. Spikes and dwell time were binned into 2 cm spatial bins and the resulting ratemap smoothed with a Gaussian kernel ($\sigma = 5$ bins). Each event ratemap was compared with the standard ratemap derived from normal track running using a Pearson correlation. As before, we established significance independently against two null distributions. First, for the event ratemap the correlation between each event and standard ratemap was percentile ranked against correlations obtained between the same ratemaps but with the standard ratemap shifted incrementally to all possible lags relative to the event ratemap. Trailing bins were wrapped around to ensure a constant number of bins were used in each comparison. We used a Wilcoxon signed-rank test to determine if the ranks observed for the grid cells differed significantly from an expected median rank of 50%. A second null distribution was generated by shifting the timing of the grid cell spikes within each replay event by a random period drawn from a flat distribution covering 0 s to the length of the replay event. Spikes that exceed the duration of the event were wrapped back to the start but otherwise the relative timing of spikes within each event was unaffected. We repeated this procedure for each event and the event ratemap constructed as before and then compared it with the standard ratemap. This entire procedure was repeated 100 times for each grid cell and in each case the correlation between the event ratemap and standard ratemap was percentile ranked against the correlations obtained from the shuffling procedure. Again we used a Wilcoxon signed-rank test to determine if the observed ranks exceed that expected by chance.

We identified forward and reverse replay events on the basis of the gradient of the line fit to the place cell posterior probability matrix. For outbound events, events that progressed down the track (for example, from the start of the track to the end) were categorized as forward events, while events depicting runs in the opposite direction were categorized as reverse events. The converse was true for inbound events. To assess whether grid cells were more likely to be active in forward rather than reverse events, we used a chi-square test to assess the proportion of all forward events accompanied by grid spikes (57%) against the proportion of all reverse events accompanied by grid spikes (45%). Moreover, we repeated the main AUC analysis, described earlier, for each event type to assess difference in grid–place cell coherence for forward and reverse events. Finally, as we recorded more forward events than reverse events (639 versus 315), we down-sampled the coherence scores for the forward events 100 times to equal the number of reverse event coherence scores. For each iteration of the down-sampling procedure we computed the mean forward coherence score and compared it against that for the reverse events. If the mean for 95 of 100 down-sampling iterations still exceeded that for the reverse events we deemed the obtained statistical difference between forward and reverse coherence scores not to be a confound of varying sample sizes.

To analyze the temporal synchrony between grid and place cell representations during replay events, we applied a time shift to grid cell spikes (starting at -60 ms then advancing in 5 ms steps to +60 ms). For each time shift we calculated the mean coherence between grid and place cells using the line fitting procedure. To assess whether the mean coherence varied as a function of time shift we used a repeated measures ANOVA for the forward and reverse events separately. To estimate the peak in this distribution, it was mean-normalized and fminsearch (Matlab 2015a, Mathworks) used to minimize the RMS difference between the data and a mean-normalized Gaussian function in which the center, height and s.d. were allowed to vary. The center of the fitted distribution was used to define the peak lag.

Finally, we compared the grid–place cell coherence exhibited by the grid cells against their directional modulation and hexagonal symmetry (i.e., gridness). The mean coherence for each grid cell estimated from all events was compared against the KL[12] divergence and modified gridness scores[16] obtained from the foraging sessions using a Spearman rank order correlation. Furthermore, we assessed the statistical significance of grid–place cell replay coherence scores for directional (KL divergence >0.15)[12] and nondirectional (KL divergence 0.15) cells separately, using the same AUC test described above. Moreover, we carried out the aforementioned time-shift analysis separately for directional and nondirectional cells as well. Finally, we also directly compared the replay coherence of the directional cells with the nondirectional cells using a two-sample t-test.

© 2016 Nature America, Inc. All rights reserved.

Statistical test. To assess place cell replay events for statistical significance we used a non-parametric spatial shuffle, described above, and percentile ranked each event against its own shuffle. Similarly, to assess grid–place cell coherence for significance we used a non-parametric area under the curve (AUC) test, using 95% confidence intervals to assess statistical significance (if the confidence interval did not contain 0 we deemed a result significant). For the alternative event ratemap method (see above) we used the Wilcoxon signed-rank non-parametric test. Spearman rank-order correlation was used to assess the relationships between grid–place cell coherence and gridness and directional modulation of grid cells. Finally, to assess bias for grid cell participation in forward (versus reverse) replay events we used a chi-square test. None of the described non-parametric tests make assumptions regarding normality or equality of variance.

Parametric test were only used to assess differences in grid cell rates during and outside replay events (paired *t*-test), grid–place cell coherence for directional and nondirectional cells (independent samples *t*-test), and variation in grid–place cell coherence across different grid cell time shifts (repeated measures ANOVA). Data distributions for these tests were assumed to be normal but this was not formally tested.

All tests were two-sided. No statistical methods were used to predetermine sample sizes but our sample sizes are similar to those reported in previous publications[6,7].

Histology. Rats were anesthetized (4% isoflurane and 4 L per min O_2), injected intraperitoneally with an overdose of Euthatal (sodium pentobarbital) after which they were transcardially perfused with saline followed by 4% paraformaldehyde solution (PFA) in phosphate buffered saline (PBS). Brains were carefully removed and stored in 4% PFA–PBS, which was exchanged for 4% PFA–PBS with 20% sucrose 2–3 d before sectioning. Subsequently, 40–50 µm frozen coronal sections were cut using a cryostat, mounted on gelatin-coated glass slides and stained with cresyl violet. Images of the sections were acquired using a Leica microscope (DM5500). Sections in which clear tracks from tetrode bundles could be seen were used to determine the locations of cells recorded.

Data and code availability. The data that support the findings of this study are available from the corresponding authors upon request. Analysis software novel to this study can been found in the **Supplementary Software** file.

A **Supplementary Methods Checklist** is available.

14. Barry, C., Hayman, R., Burgess, N. & Jeffery, K.J. *Nat. Neurosci.* **10**, 682–684 (2007).
15. Wills, T.J., Cacucci, F., Burgess, N. & O'Keefe, J. *Science* **328**, 1573–1576 (2010).
16. Langston, R.F. *et al. Science* **328**, 1576–1580 (2010).
17. Sargolini, F. *et al. Science* **312**, 758–762 (2006).

© 2016 Nature America, Inc. All rights reserved.

doi:10.1038/nn.4291